HHS Public Access

Author manuscript

Photochem Photobiol. Author manuscript; available in PMC 2020 September 04.

Published in final edited form as:

Photochem Photobiol. 2019 January ; 95(1): 419–429. doi:10.1111/php.13066.

A Combination of Visudyne and a Lipid-Anchored Liposomal Formulation of Benzoporphyrin Derivative Enhances Photodynamic Therapy Efficacy in a 3D Model for Ovarian Cancer

Imran Rizvi[1], **Shubhankar Nath**[1], **Girgis Obaid**[1], **Mustafa Kemal Ruhi**[1,3], **Kaitlin Moore**[1], **Shazia Bano**[1], **David Kessel**[2,¶,*], **Tayyaba Hasan**[1,¶,*]

[1]Wellman Center for Photomedicine, Massachusetts General Hospital and Harvard Medical School, Boston, Massachusetts, USA

[2]Department of Pharmacology, Wayne State University School of Medicine, Detroit, Michigan, USA

[3]Institute of Biomedical Engineering, Bogazici University, Istanbul, Turkey

Abstract

A major objective in developing new treatment approaches for lethal tumors is to reduce toxicity to normal tissues while maintaining therapeutic efficacy. Photodynamic therapy (PDT) provides a mechanistically-distinct approach to treat tumors without the systemic toxicity of chemotherapy drugs. PDT involves the light-based activation of a small molecule, a photosensitizer (PS), to generate reactive molecular species (RMS) that are toxic to target tissue. Depending on the PS localization, various cellular and subcellular components can be targeted, causing selective photodamage. It has been shown that targeted lysosomal photodamage followed by, or simultaneous with, mitochondrial photodamage using two different PS results in a considerable enhancement in PDT efficacy. Here, two liposomal formulations of benzoporphyrin derivative (BPD): 1. Visudyne (clinically-approved) and 2. an in-house formulation entrapping a lipid-conjugate of BPD, are used in combination to direct PS localization to mitochondria, endoplasmic reticulum and lysosomes, enabling simultaneous photodamage to all three organelles using a single wavelength of light. Building on findings by our group, and others, this study demonstrates, for the first time in a 3D model for ovarian cancer, that BPD-mediated photodestruction of lysosomes and mitochondria/ ER significantly enhances PDT efficacy at lower light doses than treatment with either PS formulation alone.

Graphical Abstract

A combination of Visudyne and a lipid-anchored liposomal formulation of benzoporphyrin derivative enhances photodynamic therapy efficacy.

*Corresponding authors': dhkessel@med.wayne.edu (David Kessel) and thasan@mgh.harvard.edu (Tayyaba Hasan).
¶Equal contribution
†This article is part of a Special Issue celebrating Photochemistry and Photobiology's 55th Anniversary

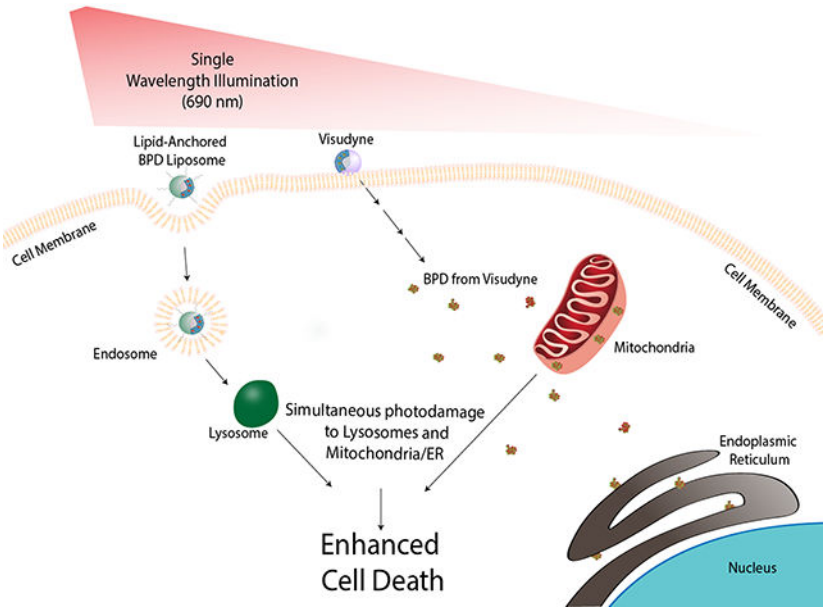

Keywords

Photodynamic therapy (PDT); dual photosensitizer; lysosomal photodamage; mitochondrial photodamage; lipid-anchored; benzoporphyrin derivative; Visudyne; liposome; ovarian cancer; 3D tumor model

Introduction

Photodynamic therapy (PDT) involves the activation of a photosensitizer (PS) with light of an appropriate wavelength to generate cytotoxic reactive molecular species (RMS)(1–4). The highly reactive nature of these RMS leads to damage within nanometers of the site of PS photoactivation. Depending, in part, on PS localization and the light dose, a range of stromal and sub-cellular sites can be targeted for photodestruction, eliciting various death modes that have been investigated (2, 5–16). Common key targets in PDT include the following sub-cellular organelles that are involved in energy production, protein trafficking and degradation/recycling: 1.) Mitochondria - important bioenergetic, biosynthetic, and stress sensing organelles (17, 18); 2.) The endoplasmic reticulum (ER) – the major site of protein folding and trafficking in the cell, which can be disrupted under adverse microenvironmental conditions such as oxidative stress and high metabolic demand, resulting in “ER stress” (19, 20); and lysosomes – acidic organelles that degrade and recycle cellular components, and are involved in lysosomal-mediated cell death pathways (21).

PDT protocols that combine PS in order to enhance efficacy have been explored by our groups and others (6, 11, 12, 22–30). These protocols exploit differences in the localization properties, and mechanisms of action, of each agent to improve PDT efficiency. Among the earliest reports (23) used a combination of (i) 5-ethylamino-9-diethylaminobenzo[a] phenothiazinium chloride (EtNBS), to damage tumor cells directly with minimal effects on vasculature, and (ii) benzoporphyrin derivative monoacid ring A (BPD-MA), with the intent

to induce vascular occlusion as well as some cellular damage. The animal model used in this study was a subcutaneous EMT-6 murine sarcoma syngeneic to BALB/c mice, treated when the tumors reached a thickness of ~1cm. Two weeks after PDT, a dramatic (>90%) reduction in tumor weight was observed only in mice treated with the combination protocol. Most (76%) of the tumors in the combination PDT group were non-measurable. Activation of EtNBS (652nm) followed by activation of BPD (690nm) was more effective than the reverse sequence. This was the first demonstration of a PDT protocol using two PS to eradicate large tumors in vivo. Importantly, treatment with either PS alone at twice the energy density and twice the PS concentration produced either no significant reduction in tumor weight or significant increase in treatment-related toxicities.

More recent studies have supported the benefits of PDT protocols combining rationally-selected PS, and investigated the mechanisms involved in improved treatment response (11, 12, 24, 26, 27, 29–33). Low-level lysosomal photodamage with N-aspartyl chlorin e6 (NPe6) followed by, or concomitant with, mitochondrial photodamage using BPD, significantly enhances PDT efficacy at lower light doses than with either PS alone (11, 12). Additional studies have demonstrated that PDT with a combination of PS can alter cytoskeletal components and influence death mechanisms (24, 29, 30).

Recently, simultaneous photodamage to lysosomes and mitochondria/ER using a single wavelength of light was investigated in ovarian cancer cells in monolayer (27). This simultaneous targeting of both the mitochondria/ER and the lysosomes was achieved by combining two liposomal preparations: one entrapping BPD and one incorporating a lipidated phosphocholine (lipid-anchored) variant of BPD (Figure 1A–B). It was found that the entrapped BPD formulation led to subcellular accumulation in mitochondria/ER, as is consistent with the Visudyne formulation and free BPD. The lipid-anchored BPD formulation was confined to lysosomes and exhibited no evidence of time-dependent or light-dependent relocalization. In treatment response studies, a synergistic enhancement of PDT efficacy with simultaneous targeting of lysosomes and mitochondria using a single wavelength of light was demonstrated in cells in monolayer. The current study demonstrates the efficacy of simultaneously targeting lysosomes and mitochondria/ER using lipid-anchored and entrapped liposomal preparations of BPD, respectively, in a 3D model for ovarian cancer, which introduces barriers to agent delivery, illumination and efficacy that are often deficient in monolayer cultures.

Materials and Methods

Cell line

Human ovarian carcinoma cells NIH:OVCAR5 (OVCAR5) were obtained from Fox Chase Cancer Center (Philadelphia, PA, USA). Cells were grown in RPMI 1640 medium (Mediatech Inc., Herndon, Virginia, USA) supplemented with 10% (v/v) heat inactivated FBS (GIBCO Life Technologies, Grand Island, New York, USA), 100 U/mL penicillin, and 100 μg/mL streptomycin. OVCAR5 cells were maintained as 2D monolayer in T75 flask at 37°C in a humidified incubator with 5% CO_2. All the cells used in this study were tested for *Mycoplasma* contamination using MycoAlert™ PLUS Kit (Lonza, LT07–710). Cell stocks were replaced when the passage number exceeded 25.

To generate OVCAR5-mCherry cells, wild-type OVCAR5 cells were transduced with lentiviruses encoding an mCherry gene. Third generation mCherry transfer plasmid pLV-mCherry (Addgene 36084), viral envelope plasmid pMD2.G (Addgene 12259), and viral packaging plasmid psPAX2 (Addgene 122260) were mixed at a molar ratio of 2:1:1 and transfected into Lenti-X™ 293T packaging cell line (TaKaRa Clontech, 632180) using X-fect transfection reagent (TaKaRa Clontech, 631317) following manufacturer's instruction. Viral supernatant was harvested 48 hours post-transfection and concentrated using Lenti-X™ Concentrator (TaKaRa Clontech, 631231). OVCAR5 cells were transduced with the viral suspension at different multiplicity of infection (MOI) in the presence of 6 μg/ml hexadimethrine bromide (polybrene, Sigma H9268). After 48 hours of transduction, cells were sorted for mCherry fluorescence using FACSaria.

3D cell culture

3D OVCAR5 nodules were grown and maintained for 11 days on Growth Factor Reduced (GFR) Matrigel (Corning 354230, lot # 7016289) beds. GFR Matrigel was thawed overnight on ice. Matrigel beds were prepared by plating 250 μL of Matrigel solution on pre-chilled 24-well black-wall plate (Krystal 24 Well Microplate or Greiner Bio-One 24-well glass bottom Sensoplate). Matrigel beds were polymerized by incubating at 37°C for 20–25 minutes. OVCAR5-mCherry cells grown in monolayer were washed with PBS and trypsinized. Cells were counted and plated at a density of 10,000 cells/well in 1 mL of 2% GFR Matrigel-containing complete growth medium as described previously (34). 3D cultures were maintained at 37°C in an atmosphere of 5% CO_2. The growth media was replaced every 3 and 6/7 days.

Chemicals and supplies

All lipids 1-palmitoyl-2-hydroxy-sn-glycero-3-phosphocoline (16:0 Lyso PC), 1,2-Dipalmitoyl-sn-glycero-3-phosphocholine (DPPC), 1,2-dioleoyl-3-trimethylammonium-propane (chloride salt) (DOTAP), 1,2-distearoyl-sn-glycero-3-phosphoethanolamine-N-[methoxy(polyethyleneglycol)-2000 (DSPE-mPEG$_{2000}$) were obtained from Avanti Polar Lipids, 4-(dimethylamino) pyridine (DMAP), N, N-Diisopropylethylamine (DIPEA) from Sigma-Aldrich, and Methanol, Dichloromethane (DCM) and Chloroform were purchased from Fisher scientific, and Verteporfin (Benzoporphyrin; BPD) was purchased from U.S. Pharmacopeia.

Preparation and Characterization of Lipid-Anchored BPD, Respective Liposomes and Visudyne

Benzoporphyrin derivative (BPD, verteporfin; mixed isomers, >94% purity) was used as provided by the manufacturer. The photosensitizer BPD was anchored to the phospholipid 1-palmitoyl-2-hydroxy-sn-glycero-3-phosphocholine (16:0 Lyso PC) using a previously published method (27). Briefly, 16:0 Lyso PC (495.63 g/mol), BPD (718.79 g/mol), 1-ethyl-3- (3dimethylaminopropyl) carbodiimide (EDC,155.24 g/mol), 4-(dimethylamino) pyridine (DMAP,122.17 g/mol), and N,N-Diisopropylethylamine (DIPEA,129.24 g/mol) were dissolved in anhydrous dichloromethane (DCM) in a molar ratio of 1:5:50:25:60 and stirred at 2500rpm for 72 hours in the dark. The 16:0 lyso PC anchored BPD (16:0 BPD-PC) was purified using preparative Thin Layer Chromatography (TLC) silica plate (Sigma-

Aldrich), running on a mobile phase of 10% methanol in DCM. Finally, pure, 16:0 Lyso PC-BPD was analyzed using matrix-assisted laser desorption/ionization (MALDI) using 2,5-dihydroxybenzoic acid (DHB) as a matrix and the UV-Visible absorption spectrum (ε_{687nm} = 34,895 $M^{-1}.cm^{-1}$) was used to quantify the concentration of BPD equivalent. The purity of the 16:0 Lyso PC-BPD conjugate was quantified by a high- performance liquid chromatography HPLC using a mobile phase gradient of 95/5 water/acetonitrile (0.1% TFA) to 5/95 water/acetonitrile (0.1% TFA) over 30 minutes. A 30-minute hold at 5/95 water/acetonitrile (0.1% TFA) was then used to elute the 16:0 Lyso PC-BPD.

Cholesterol-free 16:0 lyso PC-BPD (lipid-anchored BPD) liposomes were prepared by the thin film hydration technique under dark conditions and were designed to be moderately cationic to promote cellular uptake (27). 1,2-Dipalmitoyl-sn-glycero-3-phosphocholine (DPPC), 1,2-dioleoyl-3-trimethylammonium-propane (DOTAP), 1,2-distearoyl-sn-glycero-3-phosphoethanolamine-N-[methoxy(polyethyleneglycol)-2000 (DSPE-$mPEG_{2000}$) were mixed at a mole % ratio of 89:7.9:3.1 and doped with 0.6 mol% of 16:0 Lyso PC-BPD. Thin lipid films were formed by drying the lipid mixtures under gentle nitrogen gas flow and storing under vacuum overnight. Thin lipid films were hydrated with PBS (without calcium and magnesium) and were subjected to 5 freeze-thaw cycles consisting of 10 minutes incubation at 42–45°C (in a darkened water bath), 30 seconds of vortexing and 5 minutes incubation in ice. Multilamellar liposome vesicles of the above dispersion were sequentially extruded 11 times through two polycarbonate extrusion membranes (Whatman;100nm) using a mini-extruder system (Avanti Polar Lipids) and were dialyzed at 4°C, against PBS for 24 hours, using a Float-A-Lyzer®G2 dialysis membrane (MWCO: 300kD).

Visudyne (Bausch + Lomb) is a clinical liposomal formulation of BPD consisting of egg phosphatidylglycerol, dimyristoyl phosphatidylcholine, ascorbyl palmitate and butylated hydroxytoluene. A clinical preparation of Visudyne was prepared by hydrating the lyophilized cake in sterile PBS to an initial concentration of approximately 2 mg/ml. The BPD equivalent concentration in the lipid-anchored BPD liposomes and Visudyne was quantified using absorption spectrophotometry (ε_{687nm} = 34,895 $M^{-1}.cm^{-1}$). Hydrodynamic diameters and ζ-potentials of liposome were measured using a Zetasizer Nano ZS Dynamic Light Scattering Instrument (Malvern Instruments, Ltd., Houston, TX).

PDT Protocols

PDT efficacy was evaluated using Visudyne reconstituted in sterile PBS, lipid-anchored BPD liposomes in PBS (27), or a combination of the two agents. Based on previously published studies (27, 35–37), 3D cultures were incubated with 1 μM BPD equivalent at 37°C for either 1.5 hours (Visudyne) or 24 hours (lipid-anchored). For the combination treatment, the lipid-anchored BPD liposomes were added on day six post-plating. Following incubation for 24 hours, the medium containing lipid-anchored BPD was aspirated and replaced with medium containing Visudyne and incubated for additional 1.5 hours. Sham medium changes were done in controls and treatment groups using the individual formulations (Visudyne or lipid-anchored BPD liposomes). Prior to light irradiation, PS-containing media was aspirated and replaced with fresh complete growth medium. The wells were then irradiated using a 690nm diode laser (Model 7404, Intense Inc., North Brunswick,

NJ) at an irradiance of 50 mW/cm^2. Energy densities ranging from 0–60 J/ cm^2 were evaluated. Treatment response was evaluated on day 11.

Evaluation of Treatment Response

Results were evaluated by measuring mCherry fluorescence emitted from live cells. On day 11, mCherry fluorescence was used to quantify live tumor area on the Operetta CLS High Content Image Analysis System (Perkin Elmer) (Excitation: 530–560 nm; Emission: 570–650 nm). Images were acquired using a 5X air objective (0.16 N.A.) in a 2-by-2 mosaic-format (512×512 pixels each with 10% overlap) in 10–14 z-stacks with 50 μm step size while maintaining the temperature at 37°C with 5% CO_2. For image analysis, the Harmony 4.6 software (Perkin Elmer) was used. Image mosaics were stitched together for each plane and then multiple z-plane images were transformed into a 2-dimensional 'maximum intensity projection' (MIP) to get a global image for each well. Thresholding for mCherry fluorescence was done based on the 'no treatment control' to determine the 'live tumor area'. Tumor areas in the treated groups were normalized to respective no treatment controls.

In order to verify mCherry fluorescence as a reporter of treatment response, we conducted experiments in monolayer with OVCAR5 wild-type and mCherry expressing cells. PDT was performed using the same protocol for both wild-type and mCherry and viability was assessed by MTT assay (Figure 3A). We created a panel of images depicting mCherry response to PDT (Figure 3B). Viability data corresponds to mCherry PDT response evaluated by both MTT and Harmony 4.6 image analysis (Figure 3C–D).

Statistical Analysis

One-way analysis of variance (ANOVA) was followed by Dunnett's multiple comparison test using GraphPad Prism 7. Statistically significantly different groups were labeled corresponding to the p values. Treatment groups were internally normalized to respective no treatment controls, and results are reported as median ± 95% confidence interval (CI). All graphs represent data acquired from at least 3 independent experiments in triplicate for each group.

Results

Formulation of stable lipid-anchored BPD liposomes and Visudyne

The 16:0 Lyso PC-BPD conjugate (lipid-anchored BPD) was prepared using Steglich esterification and was confirmed to exhibit one significant peak at 1194.838 m/z using MALDI spectral analysis. The purity of the 16:0 Lyso PC-BPD conjugate was found to be 98.39% at a retention time of 36.25 minutes. Mildly cationic DPPC liposomes entrapping the 16:0 Lyso PC-BPD conjugate were prepared as described to promote endo-lysosomal uptake. Dynamic light scattering determined that the liposomes had a mean hydrodynamic diameter of 106.1 ± 0.515 nm and a polydispersity index of 0.063 ± 0.001 (mean ± S.D.). ζ-potential measurements of the lipid-anchored BPD liposomes verified their moderately cationic charge at 12.57 ± 1.3 mV (mean ± S.D.). Visudyne was prepared by reconstitution in sterile PBS as described in the Methods section. Mean hydrodynamic diameter,

polydispersity index and ζ-potential measurements of Visudyne formulation are 524.8nm ± 547.5, 0.877 ± 0.217 and 0.155 mV± 0.210, respectively (mean ± S.D.) (Figure 1C).

Figure 1 is a diagrammatic representation of Visudyne (A) entrapping the hydrophobic BPD PS molecules in a conventional egg phosphatidylglycerol based liposome and the moderately cationic, PEG coated lipid-anchored BPD liposomes (B) formed of DPPC, with a table characterizing the purity and molecular weight of the PS molecules, in addition to the ζ potential, polydispersity index, and mean hydrodynamic diameter of the formulations (C).

Evaluation of Visudyne PDT efficacy in wild-type and mCherry-OVCAR5 cells by imaging and by MTT

OVCAR5 cells expressing mCherry were sorted by FACS and were collected for use in subsequent experiments. Fluorescence was confirmed in mCherry expressing cells by imaging, whereas the wild-type cells were dark both in 2D (Figure 2A) and 3D cultures (Figure 2B) using the same acquisition parameters.

PDT dose response in wild-type and mCherry OVCAR5 cells was evaluated in monolayer (Figure 3) by fluorescence (Figures 3C and 3D) and by MTT assay (Figure 3E). Response to Visudyne PDT in mCherry OVCAR5 cells is not significantly different from wild-type OVCAR5 cells (Figure 3A). A dose-dependent decrease in mCherry fluorescence was observed (Figures 3C and 3D), and showed a similar trend to PDT efficacy evaluated by the more conventional MTT assay (Figure 3E).

PDT with combination Visudyne and a lipid-anchored BPD liposome significantly enhances efficacy relative to individual therapies in a 3D tumor model

To evaluate the efficacy of Visudyne PDT alone, 3D cultures were incubated with 1.0 μM BPD equivalent for 90 minutes, on day 7 post-plating. Following the incubation period, the medium was aspirated and replaced with fresh culture medium. Based on previous studies (27, 35–37), the tumors were irradiated with energy densities ranging from 0.5 to 10 J/cm^2 at an irradiance of 50 mW/cm^2. Consistent with historical results in wild-type OVCAR5 3D cultures (35–37), a PDT dose product of 5 μM * J/cm^2 (1.0 μM BPD x 5 J/cm^2) reduced the fraction tumor area to 0.56 (95% CI = 0.72, 0.33, $p<0.0001$). No significant reduction in fraction tumor area was seen at 0.5 J/cm^2 (1.09, 95% CI = 1.14, 1.00) or at 2.5 J/cm^2 (0.97, 95% CI = 1.17, 0.83). A modest significant increase in tumor area was observed at 1.0 J/cm^2 (1.13, 95% CI = 1.21, 1.07, $p<0.05$). At the highest energy density evaluated for Visudyne PDT in this model (10 J/cm^2), a significant reduction in fraction tumor area was observed (0.25, 95% CI = 0.30, 0.07, $p<0.0001$). Fraction tumor area in the light only (10 J/cm^2) and BPD only groups were not significantly different from no treatment controls.

A similar protocol was followed to determine PDT efficacy using the lipid-anchored BPD liposome in 3D cultures (Figure 5). Based on previously published data (27), a longer incubation period (24 hours) and substantially higher energy densities (10 – 60 J/cm^2 at 50 mW/cm^2) were used for these experiments, compared to all other experiments in this study. To keep the day of light irradiation consistent, 1.0μM BPD equivalent of lipid-anchored BPD liposome was added to the 3D cultures on day 6 post-plating (Figure 5A). The medium containing lipid-anchored BPD liposomes was aspirated after 24 hours and replaced with

fresh complete medium immediately before light irradiation (Figures 5B–D). The medium changes were staggered to adjust for the long irradiation times. As shown in the panel of representative mCherry fluorescence images (Figure 5B) and the corresponding plot (Figure 5C), PDT with lipid-anchored BPD liposomes resulted in no significant reduction in fraction tumor area at energy densities ranging from 10 J/cm^2 (the highest dose used in the Visudyne PDT experiments) to 40 J/cm^2. A significant but modest reduction in fraction tumor area was seen at an energy density of 50 J/cm^2 (0.82, CI = 0.86, 0.64, $p<0.001$). A 20% increase in the light dose (to 60 J/cm^2) produced only a small improvement in efficacy (median fraction tumor area 0.74, CI = 0.82, 0.55, $p<0.0001$). No significant toxicity was observed with the lipid-anchored BPD liposomes alone (0 J/cm^2), relative to no treatment controls.

Previous studies have demonstrated the benefits of combining PS in order to enhance PDT efficacy (6, 11, 12, 22–30) including a recent article that showed PDT with a combination of liposomes entrapping native BPD and liposomes entrapping lipid-anchored BPD significantly enhances efficacy relative to either formulation alone in monolayer culture (27). Based on these findings, the present study sought to evaluate the therapeutic benefit of combining a clinical formulation of BPD, Visudyne, and lipid-anchored BPD liposomes to enhance PDT efficacy in a 3D model. Based on previous publications (6, 11, 12, 22–30) and the dose-response curves of the individual PS formulations established in the present study, the range of light doses used for the combination protocol was 1.0 – 5.0 J/cm^2 at 50 mW/cm^2 (Figure 6). For the combination experiments, 1.0 μM BPD equivalent of lipid-anchored BPD liposome and 1.0 μM BPD equivalent of Visudyne were incubated sequentially. Specifically, the medium containing lipid-anchored BPD liposomes (1 μM BPD equivalent) was added to the 3D cultures on day 6 and then aspirated 24 hours later. Visudyne-containing medium (1 μM BPD equivalent) was then added for 90 minutes on day 7 (Figure 6A). Simultaneous incubation of lipid-anchored BPD and Visudyne, where Visudyne-containing media was added to cells without prior removal of the lipid-anchored formulation, was also evaluated in only two independent experiments in triplicate, with similar results (data not shown). Prior to light irradiation, the PS was removed and replaced with fresh complete growth medium. The representative mCherry fluorescence images in Figure 6B and the corresponding plot in Figure 6D show that PDT with a combination of Visudyne and lipid-anchored BPD liposomes significantly enhances treatment response relative to either PS formulation alone (Figures 4 and 5). Using energy densities comparable to, or substantially lower than, those used for the individual PS formulations, a significant reduction in fraction tumor area was observed in all wells that received PDT with the combination of Visudyne and lipid-anchored BPD liposomes. At light doses of 1 and 1.5 J/cm^2, reduction in fraction tumor area was significant, albeit highly variable, (median fraction tumor area: 0.54, CI = 1.02, 0.33 and 0.10, CI = 0.74, 0.08, respectively, $p<0.0001$). This variability in response decreased with increasing light dose and the median fraction tumor area following PDT with the combination of Visudyne and lipid-anchored BPD liposomes was reduced to 0.03 (CI = 0.06, 0.03, $p<0.0001$) at an energy density of 5 J/cm^2. A PDT dose product of 5 μM * J/cm^2 (2 μM BPD equivalent administered x 2.5 J/cm^2) with the combination protocol reduced median fraction tumor area to 0.09 (CI = 0.23, 0.05, $p<0.0001$). A comparable dose product with Visudyne PDT (1 μM BPD equivalent

administered x 5 J/cm^2) (Figure 4D) resulted in a median fraction tumor area of 0.56 (CI = 0.23, 0.72, 0.33).

Table 1 shows the PDT dose-product that resulted in a 20% reduction in median tumor area (LD_{20}) following PDT with either Visudyne (1 μM BPD equivalent administered), lipid-anchored BPD liposomes (1 μM BPD equivalent administered), or the combination of lipid-anchored BPD liposomes and Visudyne (2 μM BPD equivalent administered). Using Visudyne as the only photosensitizing agent, a dose product of 3.6 μM * J/cm^2 was required to achieve a 20% reduction in tumor area. A dose product of 48.5 μM * J/cm^2 was required to reduce tumor area by 20% using lipid-anchored BPD liposomes as the photosensitizing agent. Using a combination of Visudyne and lipid-anchored BPD, a dose-product of 1.5 μM * J/cm^2 resulted in a 20% reduction in tumor area.

Discussion and Conclusion

Among the factors that govern selective toxicity from PDT are the spatial confinement of light, site of PS localization, and the short distances over which the RMS remain active (1, 3, 38). Above a critical photodynamic threshold dose, the RMS-induced damage leads to cell death. In the context of therapies for cancer, rational targeting of multiple tumor compartments or sub-cellular sites have been shown to enhance photodynamic efficacy (6, 11, 12, 22–30). Among the preferential sites of localization of the FDA-approved formulation of BPD used in the present study are the mitochondria and ER (1, 3, 38). Activation by light of the liposomal formulation of BPD (Visudyne) causes photodynamic disruption of the mitochondrial membrane, which triggers the release of cytochrome c, a potent initiator of cell death (38–41). Recent studies (11, 25, 26) have shown that prior or simultaneous photodamage to lysosomes using NPe6 significantly increases the effect of mitochondrial-targeted PDT. Possible mechanisms for this observation include the release of calcium ions from lysosomes following low-level photodamage. The resulting increase in calcium ions in the cytosol initiates a calpain-mediated cleavage of ATG5, an autophagy-related protein, to a truncated, pro-apoptotic form that promotes death upon damage to mitochondria/ER (27, 42, 43). Lysosomal photodamage can also trigger the release of cathepsins, that subsequently cleave the protein Bid into a truncated form, t-Bid, which translocates to the mitochondrial membrane and promotes apoptosis (12, 33, 44). The relevance of these (or other) mechanisms to the enhanced PDT response observed in the present study in 3D ovarian cancer nodules using Visudyne and lipid-anchored BPD formulations, remains to be characterized. Studies by Villanueva and colleagues have explored the effects of PDT with two PS such as ZnPc and TMPyP, which localize to the Golgi apparatus and lysosomes, respectively. The combination was highly effective and was shown to modulate cell death mechanisms and to influence cytoskeletal rearrangement, relative to PDT with the individual PS (24, 29, 30, 45).

One of the earliest studies describing the therapeutic benefits of a two-photosensitizer sequential PDT protocol was by Cincotta et al in 1996 (23), using BPD and EtNBS with the intention to target vascular and cellular tumor compartments. Interestingly, no vascular effects were observed at the PS-light interval and light doses used for BPD-PDT. Nonetheless, the tumor eradication effect of the combination PDT protocol in large sarcomas

in vivo (1 cm thick) was greater than predicted for the activating wavelengths of light (650–700nm), suggesting mechanistic cooperation between the two PS.

A recent study from our group (27) used two liposomal formulations to modulate the sub-cellular localization of BPD and target non-overlapping sub-cellular sites: 1.) a liposomal formulation of native BPD to target mitochondria/ER and 2.) a liposomal formulation of lipid-anchored BPD to target lysosomes. The positive charge on the lipid-anchored BPD liposome helps the liposomes associate with the outer surface of the cell membrane in order to be ultimately internalized via the endocytic pathway. It is well established in the literature that cationic, PEG coated liposomes are more efficiently endocytosed than neutral or anionic liposomes(46). Following endocytosis, the intact lipid-anchored BPD liposome is trafficked via endosomes that mature into lysosomes. The PS, being conjugated to a non-switchable phospholipid, remains anchored to the liposome during this process and eventually ends up trapped in lysosomes, thereby modulating (and expanding) the sub-cellular localization of BPD. Our prior work has demonstrated that this BPD anchoring behavior is unique from BPD formulated in the clinical preparation Visudyne, whereby the PS rapidly leaches out of the formulation in the presence of serum-containing media (47). The rapid dissociation of BPD from Visudyne is therefore responsible for the mitochondria/ER subcellular localization, as is typical of native BPD. An important advancement in this protocol is the use of a single wavelength of light to activate BPD while broadening the scope of photodamage from mitochondria/ER to also include lysosomes.

The current study evaluates the efficacy of this combination PDT protocol in a 3D model that restores aspects of tumor architecture and microenvironmental cues that are not present in monolayer cultures and can influence response to therapy (e.g. gradients of nutrients and oxygen that create regions of hypoxia)(48–51). The use of mCherry as a fluorescent reporter in 3D culture confers advantages in imaging and analysis, given its relatively long emission wavelength and photostability (52). Our data evaluating PDT dose response using mCherry fluorescence, and by MTT, reported comparable levels of lethality (Figure 3). External dyes for fluorescence imaging may limited by the penetration of both the light and of the dye molecules in 3D nodules, which can impact their utility in the evaluation of cell viability. mCherry is advantageous in this respect because it is expressed by all cells in the nodule, making it a potentially useful fluorescence reporter in treatment response studies in 3D tumor nodules. Key follow-up studies using this model will include evaluating the effects of various dosing schedules and multiple cycles of PDT with each of the PS formulations alone and in combination with each other. The impact of each of these sensitization strategies on tumor reduction, on their own or in combination with conventional therapeutic agents, will likely be important areas of focus for follow-up studies.

Evaluating the efficacy of using Visudyne and lipid-anchored BPD liposomes for a combination PDT protocol in animal models will be an important next step to determining the feasibility of this therapeutic approach beyond the current in vitro findings. Consequences of this approach with respect to death modes that are triggered in vivo as a result of photodamage to mitochondria, ER, and/or lysosomes are important to consider. One such death pathway that has been reported in previous studies, termed paraptosis, is associated with the formation of an extensive network of cytosolic vacuoles (27, 43), and

requires further characterization, particularly in vivo. Modulation of death modes using a combination photosensitization approach has implications not only for developing more effective PDT regimens, but also for rationally-designed combinations treatments involving conventional agents such as chemotherapy and targeted biologics. PDT with a single PS has been shown to reverse chemoresistance, to synergize with conventional therapies, and to overcome compensatory pathways in tumors (35, 36, 53–58). The potential benefits of a dual sensitization regimen within this broader therapeutic framework merits consideration.

Acknowledgements

We would like to thank Michael Pigula for his excellent technical assistance and Michael Wyler from Perkin Elmer Inc. for helping with Operetta CLS image acquisition and Harmony data analysis. This work was supported by the following grants: R00 CA175292 (to IR), K99 CA215301 (to GO), P01 CA 084203 (to TH), R01 23378, R01 CA 156177, R01 CA 160998, R01CA160098.

References

1. Celli JP, Spring BQ, Rizvi I, Evans CL, Samkoe KS, Verma S, Pogue BW and Hasan T (2010) Imaging and photodynamic therapy: mechanisms, monitoring, and optimization. Chem Rev 110, 2795–2838. [PubMed: 20353192]
2. Abrahamse H and Hamblin MR (2016) New photosensitizers for photodynamic therapy. Biochem J 473, 347–364. [PubMed: 26862179]
3. Agostinis P, Berg K, Cengel KA, Foster TH, Girotti AW, Gollnick SO, Hahn SM, Hamblin MR, Juzeniene A, Kessel D, Korbelik M, Moan J, Mroz P, Nowis D, Piette J, Wilson BC and Golab J (2011) Photodynamic therapy of cancer: an update. CA Cancer J Clin 61, 250–281. [PubMed: 21617154]
4. Spring BQ, Rizvi I, Xu N and Hasan T (2015) The role of photodynamic therapy in overcoming cancer drug resistance. Photochem Photobiol Sci 14, 1476–1491. [PubMed: 25856800]
5. Oleinick N, Morris R and Belichenko I (2002) The role of apoptosis in response to photodynamic therapy: what, where, why, and how. Photochemical & Photobiological Sciences 1, 1–21. [PubMed: 12659143]
6. Oleinick N, Nieminen A and Chiu S (2008) Cell killing by photodynamic therapy. Advances in Photodynamic Therapy: Basic, Translational and Clinical, 115–133.
7. Xue LY, Chiu SM and Oleinick NL (2001) Photochemical destruction of the Bcl-2 oncoprotein during photodynamic therapy with the phthalocyanine photosensitizer Pc 4. Oncogene 20, 3420–3427. [PubMed: 11423992]
8. Xue LY, Chiu SM and Oleinick NL (2001) Photodynamic therapy-induced death of MCF-7 human breast cancer cells: a role for caspase-3 in the late steps of apoptosis but not for the critical lethal event. Exp Cell Res 263, 145–155. [PubMed: 11161713]
9. Kessel D and Oleinick NL (2009) Initiation of autophagy by photodynamic therapy. Methods Enzymol 453, 1–16. [PubMed: 19216899]
10. Kessel D and Oleinick NL (2010) Photodynamic therapy and cell death pathways. Methods Mol Biol 635, 35–46. [PubMed: 20552338]
11. Kessel D and Reiners JJ (2014) Enhanced efficacy of photodynamic therapy via a sequential targeting protocol. Photochemistry and photobiology 90, 889–895. [PubMed: 24617972]
12. Kessel D (2016) Photodynamic therapy: Promotion of efficacy by a sequential protocol. J Porphyr Phthalocyanines 20, 302–306. [PubMed: 27528795]
13. Xue LY, Chiu SM and Oleinick NL (2003) Staurosporine-induced death of MCF-7 human breast cancer cells: a distinction between caspase-3-dependent steps of apoptosis and the critical lethal lesions. Experimental cell research 283, 135–145. [PubMed: 12581734]
14. Reiners JJ Jr., Agostinis P, Berg K, Oleinick NL and Kessel D (2010) Assessing autophagy in the context of photodynamic therapy. Autophagy 6, 7–18. [PubMed: 19855190]

15. Kessel D and Castelli M (2001) Evidence that bcl-2 is the target of three photosensitizers that induce a rapid apoptotic response. Photochem Photobiol 74, 318–322. [PubMed: 11547571]
16. Kessel D and Arroyo AS (2007) Apoptotic and autophagic responses to Bcl-2 inhibition and photodamage. Photochem Photobiol Sci 6, 1290–1295. [PubMed: 18046484]
17. Zong WX, Rabinowitz JD and White E (2016) Mitochondria and Cancer. Mol Cell 61, 667–676. [PubMed: 26942671]
18. Vyas S, Zaganjor E and Haigis MC (2016) Mitochondria and Cancer. Cell 166, 555–566. [PubMed: 27471965]
19. Cubillos-Ruiz JR, Bettigole SE and Glimcher LH (2017) Tumorigenic and Immunosuppressive Effects of Endoplasmic Reticulum Stress in Cancer. Cell 168, 692–706. [PubMed: 28187289]
20. Hotamisligil GS (2010) Endoplasmic reticulum stress and the inflammatory basis of metabolic disease. Cell 140, 900–917. [PubMed: 20303879]
21. Kreuzaler P and Watson CJ (2012) Killing a cancer: what are the alternatives? Nat Rev Cancer 12, 411–424. [PubMed: 22576162]
22. Hamblin M (2008) Advances in photodynamic therapy: basic, translational, and clinical. Artech House.
23. Cincotta L, Szeto D, Lampros E, Hasan T and Cincotta AH (1996) Benzophenothiazine and benzoporphyrin derivative combination phototherapy effectively eradicates large murine sarcomas. Photochem Photobiol 63, 229–237. [PubMed: 8657737]
24. Acedo P, Stockert JC, Canete M and Villanueva A (2014) Two combined photosensitizers: a goal for more effective photodynamic therapy of cancer. Cell Death Dis 5, e1122. [PubMed: 24625981]
25. Kessel D and Evans CL (2016) Promotion of proapoptotic signals by lysosomal photodamage: mechanistic aspects and influence of autophagy. Photochemistry and photobiology 92, 620–623. [PubMed: 27096545]
26. Kessel D (2017) Subcellular targeting as a determinant of the efficacy of photodynamic therapy. Photochemistry and photobiology 93, 609–612. [PubMed: 27935055]
27. Rizvi I, Obaid G, Bano S, Hasan T and Kessel D (2018) Photodynamic therapy: Promoting in vitro efficacy of photodynamic therapy by liposomal formulations of a photosensitizing agent. Lasers Surg Med 50, 499–505. [PubMed: 29527710]
28. Schneider-Yin X, Kurmanaviciene A, Roth M, Roos M, Fedier A, Minder EI and Walt H (2009) Hypericin and 5-aminolevulinic acid-induced protoporphyrin IX induce enhanced phototoxicity in human endometrial cancer cells with non-coherent white light. Photodiagnosis Photodyn Ther 6, 12–18. [PubMed: 19447367]
29. Villanueva A, Stockert JC, Canete M and Acedo P (2010) A new protocol in photodynamic therapy: enhanced tumour cell death by combining two different photosensitizers. Photochem Photobiol Sci 9, 295–297. [PubMed: 20221454]
30. Gyenge EB, Luscher D, Forny P, Antoniol M, Geisberger G, Walt H, Patzke G and Maake C (2013) Photodynamic mechanisms induced by a combination of hypericin and a chlorin based-photosensitizer in head and neck squamous cell carcinoma cells. Photochem Photobiol 89, 150–162. [PubMed: 22882495]
31. Kessel D and Reiners JJ Jr. (2015) Promotion of Proapoptotic Signals by Lysosomal Photodamage. Photochem Photobiol 91, 931–936. [PubMed: 25873082]
32. Kessel D, Luo Y, Mathieu P and Reiners JJ Jr. (2000) Determinants of the apoptotic response to lysosomal photodamage. Photochem Photobiol 71, 196–200. [PubMed: 10687394]
33. Reiners JJ Jr., Caruso JA, Mathieu P, Chelladurai B, Yin XM and Kessel D (2002) Release of cytochrome c and activation of pro-caspase-9 following lysosomal photodamage involves Bid cleavage. Cell Death Differ 9, 934–944. [PubMed: 12181744]
34. Anbil SR, Rizvi I, Celli JP, Alagic N, Pogue BW and Hasan T (2013) Impact of treatment response metrics on photodynamic therapy planning and outcomes in a three-dimensional model of ovarian cancer. Journal of Biomedical Optics 18, 098004. [PubMed: 24802230]
35. Rizvi I, Anbil S, Alagic N, Celli J, Zheng LZ, Palanisami A, Glidden MD, Pogue BW and Hasan T (2013) PDT dose parameters impact tumoricidal durability and cell death pathways in a 3D ovarian cancer model. Photochem Photobiol 89, 942–952. [PubMed: 23442192]

36. Rizvi I, Celli JP, Evans CL, Abu-Yousif AO, Muzikansky A, Pogue BW, Finkelstein D and Hasan T (2010) Synergistic Enhancement of Carboplatin Efficacy with Photodynamic Therapy in a Three-Dimensional Model for Micrometastatic Ovarian Cancer. Cancer Research 70, 9319–9328. [PubMed: 21062986]
37. Celli JP, Rizvi I, Evans CL, Abu-Yousif AO and Hasan T (2010) Quantitative imaging reveals heterogeneous growth dynamics and treatment-dependent residual tumor distributions in a three-dimensional ovarian cancer model. J Biomed Opt 15, 051603. [PubMed: 21054077]
38. Kessel D (2015) Apoptosis and associated phenomena as a determinants of the efficacy of photodynamic therapy. Photochem Photobiol Sci 14, 1397–1402. [PubMed: 25559971]
39. Granville DJ, Levy JG and Hunt DW (1998) Photodynamic treatment with benzoporphyrin derivative monoacid ring A produces protein tyrosine phosphorylation events and DNA fragmentation in murine P815 cells. Photochem Photobiol 67, 358–362. [PubMed: 9523536]
40. Lam M, Oleinick NL and Nieminen AL (2001) Photodynamic therapy-induced apoptosis in epidermoid carcinoma cells. Reactive oxygen species and mitochondrial inner membrane permeabilization. J Biol Chem 276, 47379–47386. [PubMed: 11579101]
41. Oleinick NL and Evans HH (1998) The photobiology of photodynamic therapy: cellular targets and mechanisms. Radiat Res 150, S146–156. [PubMed: 9806617]
42. Yousefi S, Perozzo R, Schmid I, Ziemiecki A, Schaffner T, Scapozza L, Brunner T and Simon HU (2006) Calpain-mediated cleavage of Atg5 switches autophagy to apoptosis. Nat Cell Biol 8, 1124–1132. [PubMed: 16998475]
43. Kessel D and Reiners JJ Jr. (2017) Effects of Combined Lysosomal and Mitochondrial Photodamage in a Non-small-Cell Lung Cancer Cell Line: The Role of Paraptosis. Photochem Photobiol 93, 1502–1508. [PubMed: 28696570]
44. Kessel D and Reiners JJ Jr. (2014) Enhanced efficacy of photodynamic therapy via a sequential targeting protocol. Photochem Photobiol 90, 889–895. [PubMed: 24617972]
45. Acedo P, Stockert J, Cañete M and Villanueva A (2014) Two combined photosensitizers: a goal for more effective photodynamic therapy of cancer. Cell death & disease 5, e1122. [PubMed: 24625981]
46. Miller CR, Bondurant B, McLean SD, McGovern KA and O'Brien DF (1998) Liposome-cell interactions in vitro: effect of liposome surface charge on the binding and endocytosis of conventional and sterically stabilized liposomes. Biochemistry 37, 12875–12883. [PubMed: 9737866]
47. Obaid G, Jin W, Bano S, Kessel D and Hasan T (2018) Nanolipid Formulations of Benzoporphyrin Derivative: Exploring the Dependence of Nanoconstruct Photophysics and Photochemistry on Their Therapeutic Index in Ovarian Cancer Cells. Photochem Photobiol.
48. Foster TH, Murant RS, Bryant RG, Knox RS, Gibson SL and Hilf R (1991) Oxygen consumption and diffusion effects in photodynamic therapy. Radiat Res 126, 296–303. [PubMed: 2034787]
49. Foster TH, Hartley DF, Nichols MG and Hilf R (1993) Fluence rate effects in photodynamic therapy of multicell tumor spheroids. Cancer Res 53, 1249–1254. [PubMed: 8443805]
50. Nichols MG and Foster TH (1994) Oxygen diffusion and reaction kinetics in the photodynamic therapy of multicell tumour spheroids. Phys Med Biol 39, 2161–2181. [PubMed: 15551546]
51. Rizvi I, Bulin A-L, Briars E, Anbil S and Hasan T (2016) Mind the gap: 3D models in photodynamic therapy. In Photodynamic Medicine. pp. 197–221.
52. Shaner NC, Campbell RE, Steinbach PA, Giepmans BN, Palmer AE and Tsien RY (2004) Improved monomeric red, orange and yellow fluorescent proteins derived from Discosoma sp. red fluorescent protein. Nature biotechnology 22, 1567.
53. Huang HC, Mallidi S, Liu J, Chiang CT, Mai Z, Goldschmidt R, Ebrahim-Zadeh N, Rizvi I and Hasan T (2016) Photodynamic Therapy Synergizes with Irinotecan to Overcome Compensatory Mechanisms and Improve Treatment Outcomes in Pancreatic Cancer. Cancer Res 76, 1066–1077. [PubMed: 26719532]
54. Rizvi I, Bulin A-L, Briars E, Anbil S and Hasan T (2016) Mind the Gap: 3D Models in Photodynamic Therapy. In Photodynamic Medicine: From Bench to Clinic. (Edited by Herwig Kostron TH), pp. 197–221. The Royal Society of Chemistry.

55. Spring BQ, Rizvi I, Xu N and Hasan T (2015) The role of photodynamic therapy in overcoming cancer drug resistance. Photochemical & Photobiological Sciences 14, 1476–1491. [PubMed: 25856800]

56. Anbil S, Rizvi I, Celli JP, Alagic N, Pogue BW and Hasan T (2013) Impact of treatment response metrics on photodynamic therapy planning and outcomes in a three-dimensional model of ovarian cancer. Journal of biomedical optics 18.

57. Celli JP, Rizvi I, Evans CL, Abu-Yousif AO and Hasan T (2010) Quantitative imaging reveals heterogeneous growth dynamics and treatment-dependent residual tumor distributions in a three-dimensional ovarian cancer model. Journal of biomedical optics 15.

58. del Carmen MG, Rizvi I, Chang YC, Moor ACE, Oliva E, Sherwood M, Pogue B and Hasan T (2005) Synergism of epidermal growth factor receptor-targeted immunotherapy with photodynamic treatment of ovarian cancer in vivo. Journal of the National Cancer Institute 97, 1516–1524. [PubMed: 16234565]

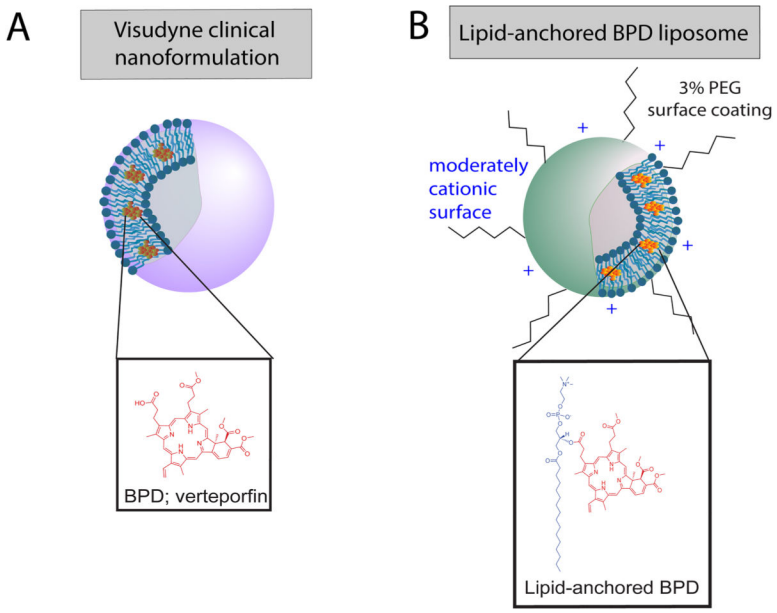

C

	Visudyne	Lipid-Anchored BPD Liposome
Characteristics	Conventional EPG Liposome	Cholesterol-free Cationic DPPC Liposome
Molecular Weight of BPD Variant (g/mol)	718.8	1194.8
Purity of Lipid-anchored BPD Conjugate	--	98.39%
Zeta Potential	0.16 mV	+12.57 mV
Polydispersity Index	0.877	0.063
Hydrodynamic Diameter	524.8nm	106.1nm

Figure 1. Structure of Visudyne and lipid-anchored BPD liposome.

A) BPD (Verteporfin, inset) PS is associated with the lipid bilayer of the liposome. BPD dissociates from the liposome upon entering the cell. B) The lipid-anchored BPD liposome formulation has a moderately cationic surface and is coated with 3% PEG. BPD is conjugated to a lipid in the bilayer of the liposome (inset). C) Characterization table of Visudyne and lipid-anchored BPD liposome. Molecular weight, ζ potential, polydispersity index, and hydrodynamic diameter are reported for each formulation. Purity is reported for the lipid-anchored BPD molecule only; the purity of BPD in the clinical Visudyne formulation is of clinical grade as used by the manufacturer.

Note: Figures are not drawn to scale.

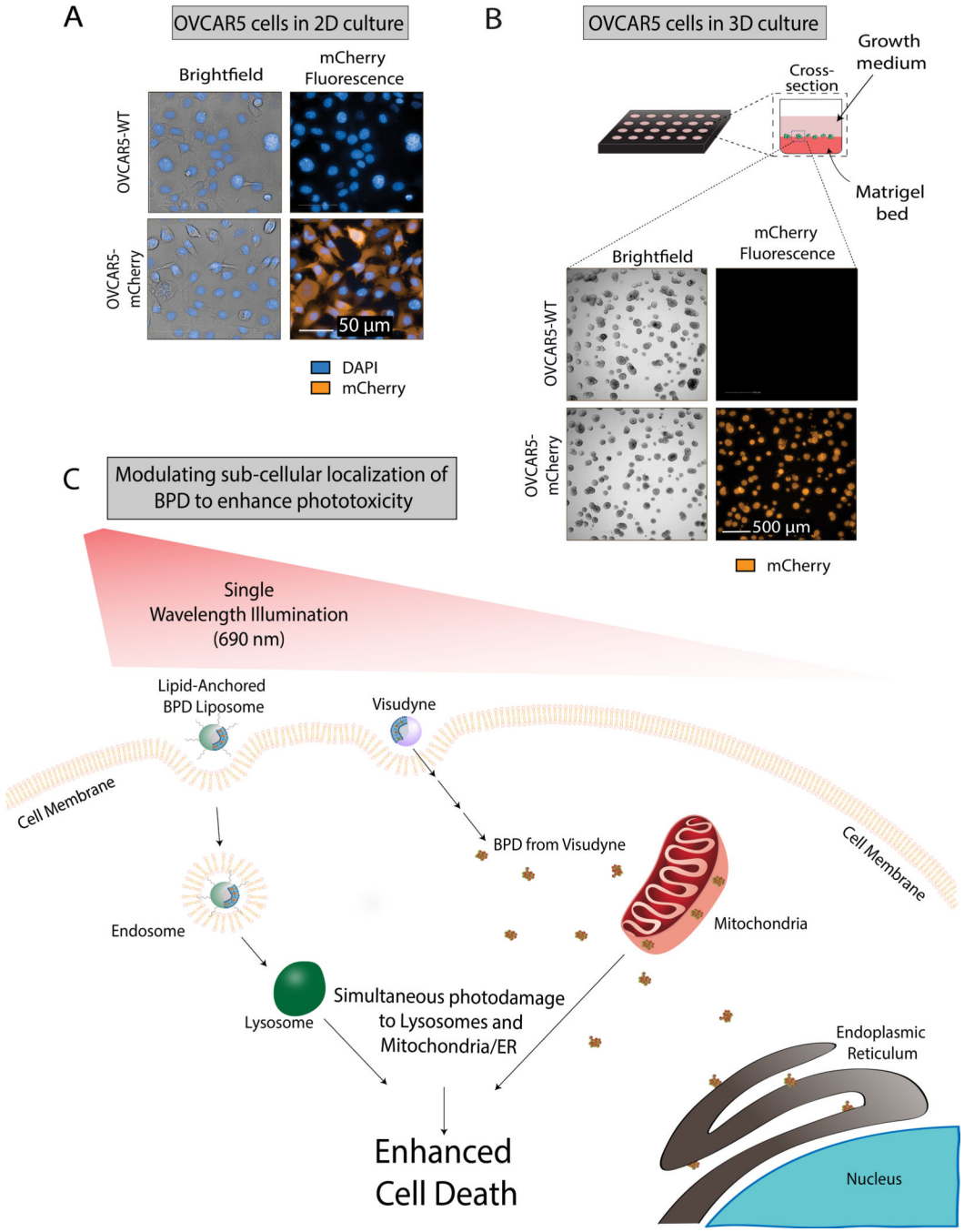

Figure 2. Schematic showing the mechanistic rationale for targeted PDT using Visudyne in combination with lipid-anchored BPD to enhance killing in monolayer and 3D Cultures of OVCAR5 mCherry and wild-type cells.

A) Comparison of fluorescence and morphology of OVCAR5 wild-type (top row) and mCherry (bottom row) cells grown in 2D. Cells were stained with DAPI (blue) and imaged for brightfield (grey) and mCherry fluorescence (orange). Scale bar: 50 µm. B) In the 3D culture model, OVCAR5 cells form nodules in growth medium on a Matrigel bed in each well of a 24-well plate. Brightfield and fluorescence images of OVCAR5 wild-type and mCherry grown in 3D are shown. Scale bar: 500 µm. C) mechanism of dual PS-mediated

phototoxicity: lipid-anchored BPD liposome is taken up by the cell membrane forming an endosome, which matures into a lysosome. The free BPD from Visudyne enters the cell and localizes primarily to the mitochondria and partially to the endoplasmic reticulum. When irradiated with a single wavelength of light, the low-level lysosomal photodamage enhances mitochondrial-related cell death pathways upon initiation of mitochondrial photodamage.

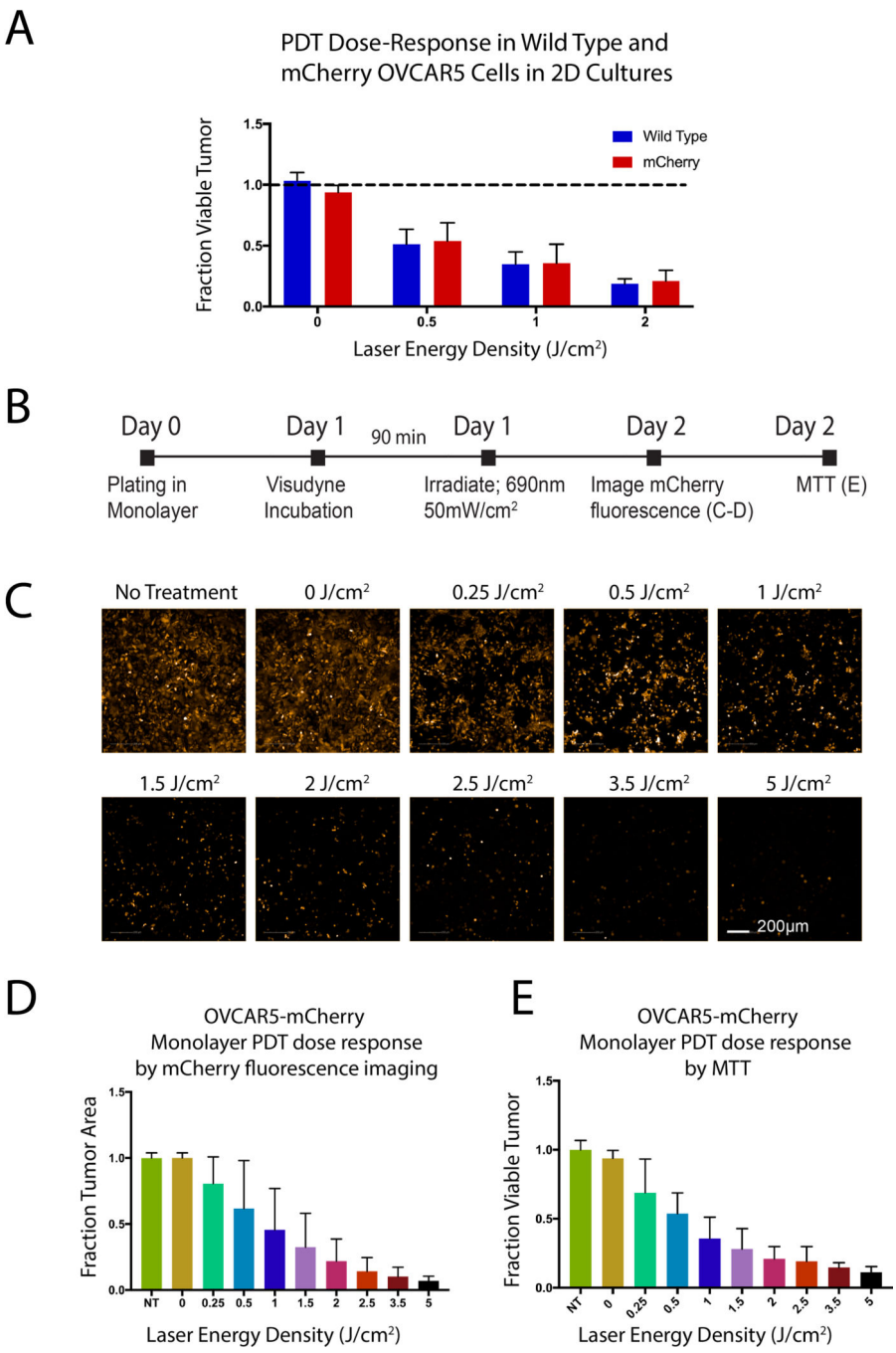

Figure 3. Efficacy of Visudyne PDT evaluated by mCherry fluorescence and by MTT in monolayer culture.

A) Response to Visudyne PDT is not significantly different between mCherry cells and OVCAR5 wild-type cells. Results were evaluated by MTT and treatment groups were normalized to respective no treatment controls. B) Experimental timeline to evaluate OVCAR5 PDT response by MTT assay and image analysis in monolayer. C) Fluorescence images showing a dose-dependent decrease in mCherry signal (Scale bar: 200 μm), which is plotted in (D). E) PDT response in mCherry OVCAR5 cells evaluated by MTT.

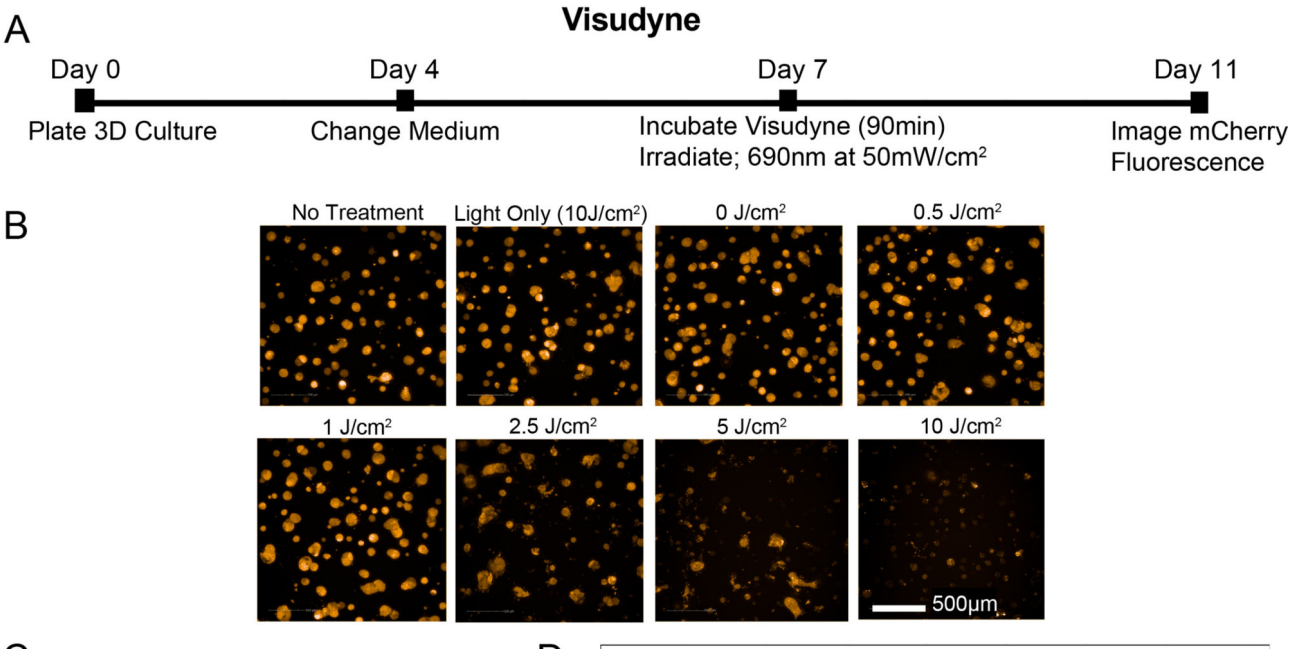

D

Visudyne PDT				
Energy Density (J/cm²)	PDT Dose Product (µM*J/cm²)	Fraction Tumor Area	Lower 95% CI	Upper 95% CI
Light only (10J/cm²)	0	0.94	0.87	0.99
BPD only (no light)	0	1.12	1.04	1.18
0.5	0.5	1.09	1.00	1.14
1	1	1.13	1.07	1.21
2.5	2.5	0.97	0.83	1.17
5	5	0.56	0.33	0.72
10	10	0.25	0.07	0.30

Figure 4. Visudyne-PDT: experimental timeline and results.

A) Eleven-day timeline for PDT experiments using Visudyne. OVCAR5-mCherry cells were plated on Matrigel on day 0 in 1mL of 2% GFR-Matrigel in RPMI complete growth medium, followed by a medium change on day 4 with 2% GFR-Matrigel in RPMI complete growth medium. Visudyne (BPD equivalent concentration of 1.0 µM) in RPMI complete growth medium (no 2% GFR-Matrigel) was added to each appropriate well, and incubated for 90 minutes before being replaced with fresh complete growth medium (with 2% GFR-Matrigel) and irradiated with a 690nm light at an irradiance of 50mW/cm^2. Cultures were imaged for mCherry fluorescence four days later, on day 11. B) A panel of representative images shows decreasing mCherry fluorescence with increasing PDT dose (scalebar: 500 µm), and the corresponding dose-response plot in (C). All data were internally normalized to respective no treatment controls, as indicated by the dashed line. Groups that are statistically significant from no treatment are labeled (*: $p < 0.05$, ***: $p < 0.001$, ****: $p < 0.0001$). All values are reported as median ± 95% CI. The table in (D) summarizes energy density (in J/cm^2), PDT dose product (in µm*J/cm^2), median fraction of tumor area remaining after treatment, and upper and lower 95% confidence intervals of the median. The PDT dose product is the energy density (in J/cm^2) multiplied by the concentration of PS administered

(μM) (in this case 1μM). All groups, except no treatment and light only, received Visudyne (1.0 μM BPD-equivalent).

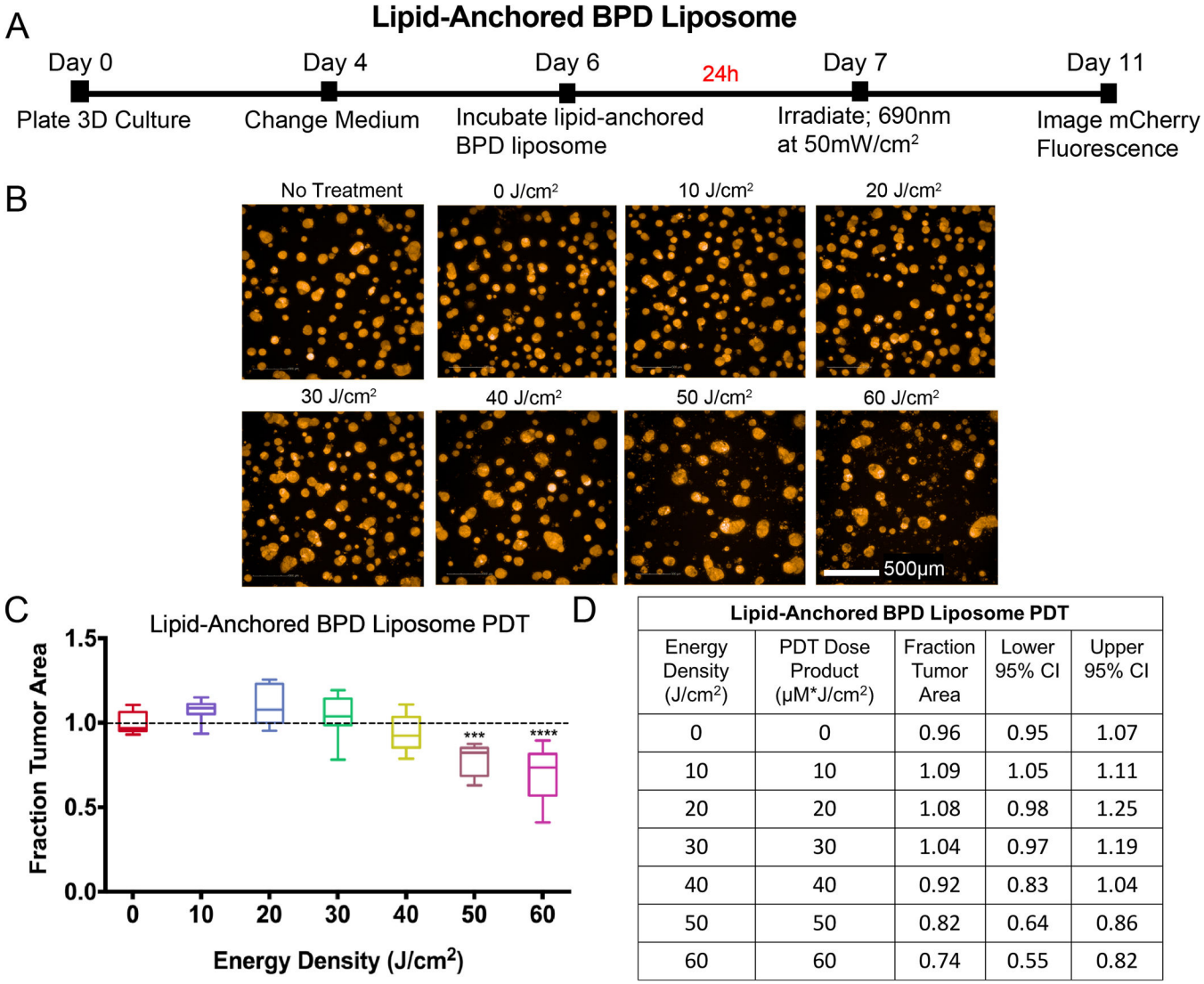

Lipid-Anchored BPD Liposome PDT				
Energy Density (J/cm²)	PDT Dose Product (µM*J/cm²)	Fraction Tumor Area	Lower 95% CI	Upper 95% CI
0	0	0.96	0.95	1.07
10	10	1.09	1.05	1.11
20	20	1.08	0.98	1.25
30	30	1.04	0.97	1.19
40	40	0.92	0.83	1.04
50	50	0.82	0.64	0.86
60	60	0.74	0.55	0.82

Figure 5. Lipid-anchored BPD liposome-PDT: experimental timeline and results.

A) Eleven-day timeline for experiments with lipid-anchored BPD liposome as the PS. On day 6, 1.0µM BPD equivalent of the formulation in growth medium was added to treatment wells and incubated for 24 hours. The PS-containing medium was removed and replaced with fresh medium, then treatment groups were irradiated on day 7. Imaging of mCherry fluorescence was performed on day 11. B) Image panel depicting mCherry fluorescence of 3D cultures treated with PDT with lipid-anchored BPD liposome. Scalebar: 500µm. C) Dose-response curve of results normalized to the no treatment control. Groups that are statistically different from no treatment were labeled according to p values. (***: $p < 0.001$, ****: $p < 0.0001$). All values are reported as median ± 95% CI and are summarized in D). Results table for lipid-anchored BPD liposome PDT. Median fraction tumor area with upper and lower 95% CI are reported. Because the PS concentration is 1µM, the PDT dose product (µM*J/cm^2) is equal to the energy density (J/cm^2). All groups received the lipid-anchored BPD liposome, including the 0 J/cm^2 group, to evaluate the toxicity of the formulation on its own.

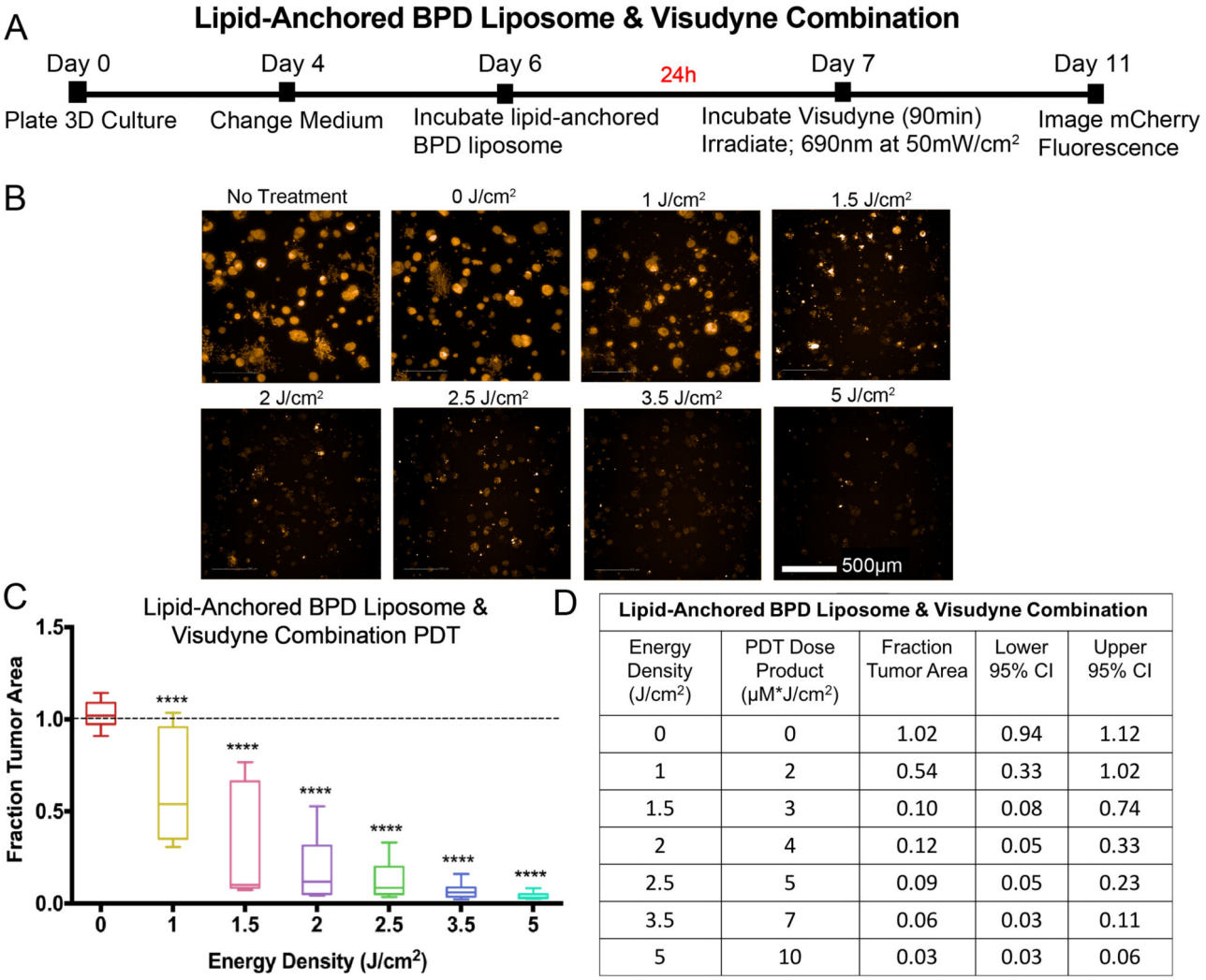

D

Lipid-Anchored BPD Liposome & Visudyne Combination				
Energy Density (J/cm²)	PDT Dose Product (µM*J/cm²)	Fraction Tumor Area	Lower 95% CI	Upper 95% CI
0	0	1.02	0.94	1.12
1	2	0.54	0.33	1.02
1.5	3	0.10	0.08	0.74
2	4	0.12	0.05	0.33
2.5	5	0.09	0.05	0.23
3.5	7	0.06	0.03	0.11
5	10	0.03	0.03	0.06

Figure 6: Combination Visudyne and lipid-anchored BPD liposome-PDT: experimental timeline and results.

A) Eleven-day timeline for PS combination experiments. 1.0µM of lipid-anchored BPS liposome was added to each treatment well on day 6 and incubated for 24 hours. PS-containing medium was removed on day 7, followed by the addition of 1µM Visudyne for 90 minutes. Irradiation was still performed on day 7 and plates were imaged on day 11. B) Panel of images of 3D cultures treated with lipid-anchored BPD liposome & Visudyne combination, at various energy densities. The images show mCherry fluorescence. C) Dose-response curve of PS combination experiments. Graph shows the energy density given (in J/cm^2) vs. median fraction tumor area, which was normalized to the no treatment control group. Groups that were statistically different from no treatment were labeled according to p values. (****: $p < 0.0001$). D) Table quantifies PDT response. In the lipid-anchored BPD + Visudyne combination, the total PS concentration is 2µM, which is represented in the PDT dose product. All groups received both Visudyne and lipid-anchored BPD liposome, including the 0 J/cm^2 group, to evaluate the toxicity of the combination alone.

Table 1:

LD_{20} for each PS formulation and their combination (Visudyne, lipid-anchored BPD, and lipid-anchored BPD + Visudyne).

LD_{20} (PDT Dose Product, μM*J/cm^2)	
Visudyne	3.6
Lipid-Anchored BPD Liposome	48.5
Lipid-Anchored BPD Liposome & Visudyne	1.5

Values in the table represent the PDT dose product that results in a 20% decrease in viability, in μM*J/cm^2.